Study of the Injection of Secondary Air into the Intake Manifold of the Gas Turbine to Avoid the Compressor Surging Phenomenon

George Iulian Balan

Defence and Security Systems Engineering, Faculty of Aircraft and Military Vehicles, Ferdinand I Military Technical Academy, Romania
george333@gmail.com

Dragos Gabriel Zisopol

Mechanical Engineering Department, Petroleum-Gas University Ploiești, Romania
zisopold@upg-ploiesti.ro (corresponding author)

Amado Stefan

Department of Integrated Aviation Systems and Mechanics, Faculty of Aircraft and Military Vehicles, Ferdinand I Military Technical Academy, Romania
amado.stefan@mta.ro

Vasile Nastasescu

Department of Integrated Aviation Systems and Mechanics, Faculty of Aircraft and Military Vehicles, Ferdinand I Military Technical Academy, Romania
vasile.nastasescu@mta.ro

Lucian Grigore

Center of Excellence in Robotics and Autonomous Systems - CERAS, Ferdinand I Military Technical Academy, Romania
lucian.grigore64@gmail.com

ABSTRACT

This paper presents part of the research on avoiding or reducing the surging effects that appear in the axial compressor intake manifold of a gas turbine. This research has led to an original solution validated by numerical simulations and experimental investigations. The increased amount of air suddenly required in the transient regime of the gas turbine is introduced into the intake manifold through slits arranged perpendicular to the direction of flow, on an aerodynamic profile at a certain angle to it and a certain distance from the minimum transversal section. The slits are arranged on the opposite sides of the gallery and connect with a transverse channel of the airfoil, in which there is air under pressure, from which the introduction of additional air is ordered. The numerical and experimental results extended to the influence of many geometric and mechanical parameters, proving that the proposed solution is as effective as possible compared to the classic ejector solution.

Keywords-gas turbine; secondary air injection; intake ducting; flow simulation

I. INTRODUCTION

The increasing use of gas turbines in vehicles and ships makes scientific research on their operation at the highest possible parameters topical. This paper presents the results of previous research on air intake, with the avoidance or reduction of the compressor surge phenomenon specific to transient regimes. The air intake in a gas turbine is a continuous process at high and variable flow rates to ensure the amount required not only for fuel combustion but also for cooling the engine components. A maximum of 10% of this air quantity can be used for auxiliary processes of the gas turbine [1-2]. This study

adopted an original solution of additional air injection, which, through numerical simulations and experimental investigations, proved to be superior to the classic solution that uses the ejection phenomenon.

Depending on the field of power plant use, the air intake ducting system is designed to ensure the amount of filtered, dehumidified, and guided air to the intake nozzle of the gas turbine. Since the supply air in gas turbines is compressed by passing successively through the compressor rotors, the main requirements regarding the quality of the air and the gas-dynamic conditions can be obtained as follows: limiting the admission of impurities [3], limiting the admission of water, except in the case where a controlled flow of water vapor is ensured to improve the efficiency of the engine or compressor washing solutions, avoiding the admission of objects between the compressor blades, avoiding the accumulation of ice in the supply path or on the air guide struts [4], and configure the gas-dynamic route to reduce losses but also to avoid the occurrence of surging conditions during transient operating regimes [5-6].

In [2, 7], a study of the airflow through the intake manifold of the ST40 engine was presented, highlighting the distribution of velocities and pressures using a CFD analysis. The results had a high degree of generality, but numerical simulation and experimental research were performed for the intake manifold of the ST40M-type gas turbine, as shown in Figure 1. In addition to the intake plenum configuration, the air guide vanes are used in the first stage of the compressor. Guide vanes can be of fixed type if the gas turbine engine works mainly at a predetermined regime, or of orientable type to achieve air guidance according to the load of the power plant. Since the amount of air required to supply gas turbines is considerably greater than the air required for diesel engine operation, intake paths with complicated configurations can generate significant gas-dynamic resistances. In [8], the pressure variation in the outlet section of the gas turbine intake manifold was analyzed according to the pressure variations produced by the wind.
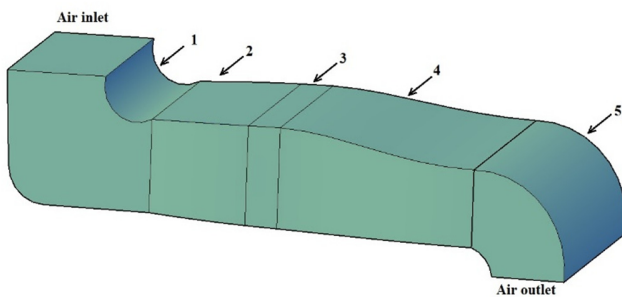

Fig. 1.   Air intake manifold sector of the gas turbine. 1 - 90 degree transition volute, 2 - intake manifold TR1, 3 – elastic couple and anti-stone sieve, 4 - intake manifold TR2, 5 - 90 degree transition volute.

For marine power plants, air intake paths for gas turbines must satisfy all the listed requirements to ensure the operation of the ship. In [9] the design and verification of the intake manifold of the gas turbine engine was addressed, where the manifold configurations were analyzed at the inlet to the turbine compressor.

II.   RESEARCH OBJECTIVES

Laboratory investigation of the phenomena specific to the transient regime of air supply was performed by injecting air into the intake manifold of a 1:4 scale model using a controlled flow compressor. The main objective of the study was the validation of the original solution of introducing additional air, which leads to superior performance compared to the classical processes. Further objectives were to investigate the influence of the geometric characteristics of the proposed solution, such as the position of the access slot in the intake manifold and the angle of the nozzle. There were also other secondary objectives regarding the geometrical and mechanical characteristics of the secondary air introduction, but having little influence, they are not presented here. This study presents the essential elements of the research performed, the results of which can be generalized to other similar constructions.

III.   NUMERICAL DETERMINATIONS

Flow simulation software was used to model airflow through the gas turbine intake manifold model, which features the ability to model laminar and turbulent flows. The Favre-averaged Navier-Stokes equations were used to predict turbulent flows, where time-averaged effects of the flow turbulence on the flow parameters were considered, whereas the other, i.e. large-scale, time-dependent phenomena were directly taken into account. Flow simulation uses transport equations for the turbulent kinetic energy and its dissipation rate [10-11]. The conservation laws for mass [12], angular momentum, and energy in the Cartesian coordinate system rotating with angular velocity about an axis passing through the coordinate system's origin can be written in the conservation form as follows:

$$\frac{\partial \rho}{\partial t} + \frac{\partial}{\partial x_i}(\rho v_i) = S_M^p \tag{1}$$

$$\frac{\partial \rho v_i}{\partial t} + \frac{\partial}{\partial x_i}(\rho v_i v_j) =$$
$$-\frac{\partial p}{\partial x_i} + \frac{\partial}{\partial x_i}(\tau_{ij} + \tau_{ij}^R) + S_i + S_{Ii}^p \tag{2}$$

$$\frac{\partial \rho H}{\partial t} + \frac{\partial}{\partial x_i}(\rho v_i H) =$$
$$\frac{\partial p}{\partial t} + \frac{\partial}{\partial x_i}(v_j(\tau_{ij} + \tau_{ij}^R) + q_i) -$$
$$\tau_{ij}^R \frac{\partial v_i}{\partial x_j} + \rho\varepsilon + S_i v_i + S_H^p + Q_H \tag{3}$$

$$H = h + \frac{v^2}{2} + \frac{5}{3}k - \frac{\Omega^2 r^2}{2} - \sum_m h_m^0 y_m \tag{4}$$

where v is the velocity of the fluid, ρ is the density, S_i is the mass-distributed external force, which can be gravitational ($S_i^{grav} = -\rho g_i$, g_i is the component of the gravitational acceleration in the i direction), porous, or inertial due to the rotation of the coordinate system, h is the enthalpy, and S_M^p, S_{Ii}^p and S_H^p are due to the interaction at the interface with the Euler-Lagrange particles. Q_H is the heat source per unit volume, τ_{ij} is the viscous stress tensor, q_i is the diffusive heat flux, Ω is the angular velocity of the mobile coordinate system in rotational motion, r is the radius from the elementary fluid particle to the

axis of rotation, k is the kinetic energy turbulence, h_m^0 is the enthalpy of the m component of the fluid mixture and y_m is the concentration of the m component of the fluid mixture [10, 13]. The stress tensor for Newtonian fluids is defined as:

$$\tau_{ij} = \mu_t \left(\frac{\partial u_i}{\partial x_j} + \frac{\partial u_j}{\partial x_i} - \frac{2}{3} \delta_{ij} \frac{\partial u_k}{\partial x_k} \right) \tag{5}$$

In the Boussinesq hypothesis, the Reynolds stress tensor has the form:

$$\tau_{ij}^R = \mu_t \left(\frac{\partial u_i}{\partial x_j} + \frac{\partial u_j}{\partial x_i} - \frac{2}{3} \delta_{ij} \frac{\partial u_k}{\partial x_k} \right) - \frac{2}{3} \rho k \delta_{ij} \tag{6}$$

where δ_{ij} is the Kronecker symbol or delta function, μ is the dynamic viscosity, μ_t is the turbulent viscosity, k is the turbulent kinetic energy, and ε is the turbulent dissipation rate [14-15]. As part of the numerical determinations, simulations were carried out in transient mode, with the operation of only the fan at maximum speed, and several simulations in stationary mode for different geometrical configurations of the secondary air collector gallery, using only air injection. Fan modeling allows the calculation of airflow through the gallery using a geometric domain as the envelope of the fan blades rotating at the fan's angular velocity. This calculation is a way to estimate the airflow flowing through the intake manifold when using the fan and secondary air injection simultaneously. The following variants were considered to estimate the influence of the effect of the introduction of compressed air on the airflow passing through the gallery:

- The variation of the outlet position of the manifold nozzle in the intake manifold compared to the entrance to the modified section (relative to the leading edge of the wall profile)

- The variation of the angle of the nozzle with respect to the longitudinal axis of the intake manifold.
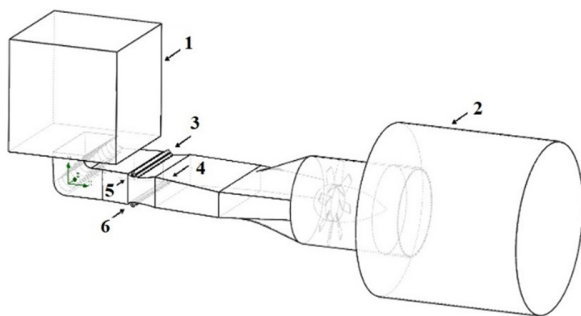

Fig. 2.   The flow domain and the boundary conditions. 1,2 – atmospheric pressure surfaces; 3, 4, 5, 6 – compressed air at 0,015 kg/s flow.

In all these simulations, the convergence of the mass flow through the exit surface of the computational domain (the base and the side surface of the cylinder at the exit of the fan) and the convergence of the default parameters were observed. The final solution was chosen according to the geometric configuration that ensured the highest flow rate of air leaving the flow domain, keeping the same static pressure of the secondary air in each case. Figure 2 shows the flow domain

used in the CFD analysis [16-17] and the position of the boundary conditions used.

A. Influence of the Nozzle Position on Air Flow through the Intake Ducting Using Only Secondary Air

The position of the nozzle outlet in the gallery was changed, starting from 30 to 60 mm from the entrance to the modified section, in 5 mm increments, to study the influence of the position between the outlet of the nozzle in the intake ducting compared to the leading edge of the modified section wall on the airflow. The reduction of the distance below 30 mm of the nozzle outlet in the manifold can no longer be achieved for the 12 mm diameter of the manifold (next to this position being the minimum section of the intake manifold) without its geometry intersecting the wall of the gas turbine intake. For these numerical determinations, for the condition of stopping the calculation, the convergence of the calculated mass flow rate on the exit surface of the domain and the total mass flow rate in addition to the usual parameters was followed. Figures 3 and 4 show the velocity field on the plane of symmetry of the gallery, in the area of the modified section, for the exit at 30 and 60 mm from the entrance to the modified section.
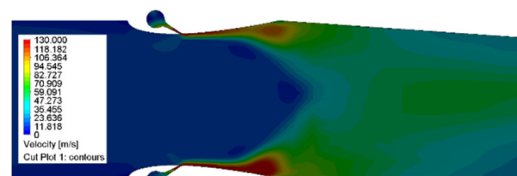

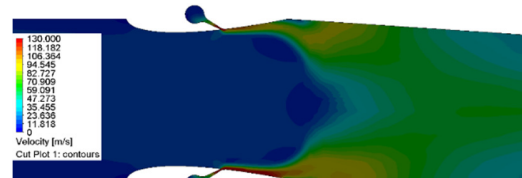Fig. 3.   Exit at 30 mm from the section entrance.

Fig. 4.   Exit at 60 mm from the section entrance.
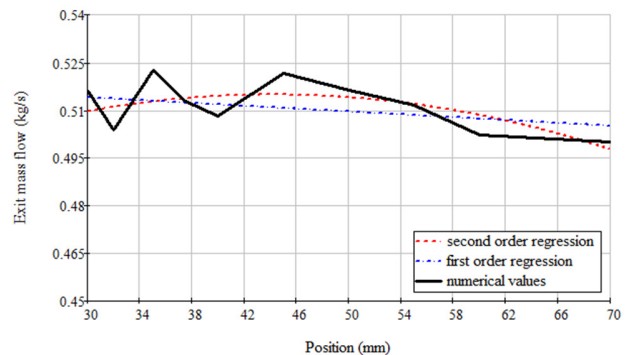

Fig. 5.   The variation of the airflow at the outlet of the gallery depending on the distance between the nozzle and the edge of the wall profile.

Figure 5 shows the variation of the mass flow rate in the exit section of the domain depending on the exit position of the nozzle in the gallery. The laws of linear regression and second order are:

$$0.521 - 2.233 \cdot 10^{-4} \cdot x_{position} \qquad (7)$$

$$0.464 + 2.296 \cdot 10^{-3} \cdot x_{position} - 2.595 \cdot 10^{-5} \cdot x_{position}^2 \qquad (8)$$

B. . Influence of Nozzle Angle on Manifold Airflow Using Only Secondary Air

To determine the influence of the angle of the channel with the axis of the gas turbine intake manifold, the geometric configuration with the 12 mm collector manifold, the outlet of the nozzle in the manifold at 35 mm from the leading edge, and the dihedral angle of the nozzle of 8° were used. The angle of inclination of the channel bisector plane relative to the horizontal was varied from 26 to 52° in increments of 2°. When the angle of inclination of the nozzle varied, the condition of its constant length was maintained. Figures 6 and 7 show the velocity field on the plane of symmetry of the gallery, in the area of the modified section, for inclination angles of 26° and 40°. Figure 8 shows the mass airflow rate in the exit section of the domain depending on the angle of the nozzle and the linear regression functions and by the least squares method. The laws of linear regression and second order are:

$$0.627 - 3.62 \cdot 10^{-3} \cdot x_{angle} \qquad (9)$$

$$0.536 + 1.261 \cdot 10^{-3} \cdot x_{angle} - 6.259 \cdot 10^{-5} \cdot x_{angle}^2 \qquad (10)$$
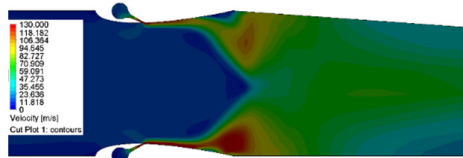

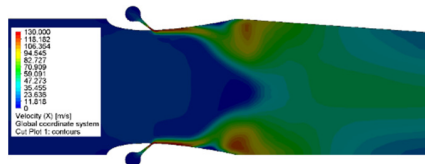Fig. 6.   The 26 degrees nozzle outlet inclination.

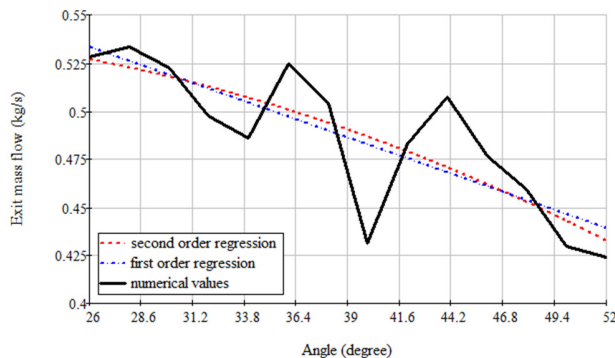Fig. 7.   The 40 degrees nozzle outlet inclination.

Fig. 8.   The variation of mass flow at the outlet of the gallery according to the angle of the nozzle.

C. Airflow Modeling Through the Modified Intake Manifold with Fan and Secondary Air Operation

The geometric configuration used corresponds to the nozzle exit position in the galley in front of the entrance to the modified section, with the angle of the nozzle axis to the longitudinal direction of the air intake manifold. The calculation was performed in transient mode, for a time interval of two seconds, an interval considered sufficient to equalize the flow through the gallery. The rotation speed of the domain containing the fan blades was 3000 rpm. The law of variation of the airflow rate for the secondary air intakes was implemented in tabular. Figures 9 and 10 show the streamlines as a function of speed and the static pressure distribution on the plane symmetry for the moment of time $t = 2$ s, respectively.

TABLE I.   TIME VARIATION OF SECONDARY AIRFLOW RATE

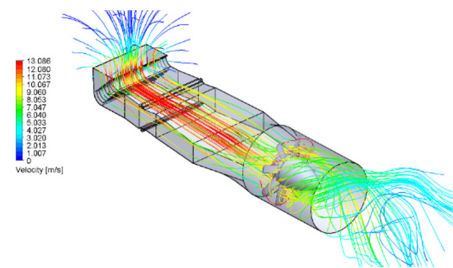| Time (s)	Mass airflow rate (kg/s)
0.0	0.000
2.0	0.000
2.1	0.015
4.0	0.015

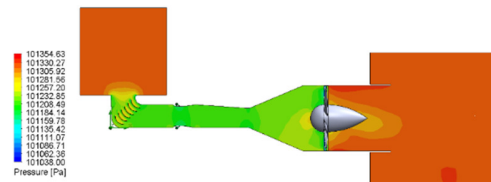Fig. 9.   Velocity distribution on streamlines at $t = 2$ s.

Fig. 10.   Pressure distribution on the symmetry plane of the gallery at $t = 2$s.

Figure 11 shows the speed distribution on the streamlines at the time of 2.4 s. The average value of the flow produced by the fan is 0.401 kg/s and after the injection of the secondary air with a total flow in the four intakes of 0.06 kg/s, an average value of 0.623 kg/s results at the exit, as shown in Figure 12.
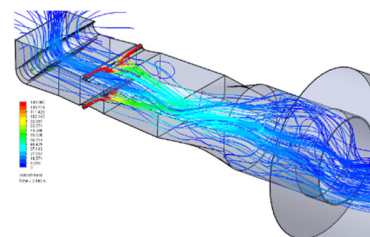

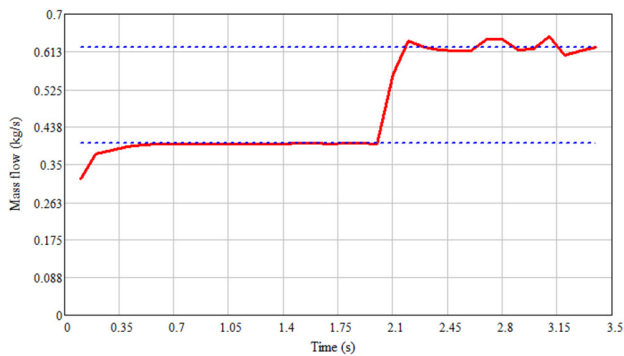
Fig. 11.   Streamlines at $t = 2.4$ s.

Fig. 12.   Time variation of the airflow at the exit of the calculation domain.

IV. EXPERIMENTAL DETERMINATIONS

Experimental determinations were carried out on a 1:4 scale 3D printed model of the intake manifold, as shown in Figure 13. The area in the gallery for which the scale model was made was chosen for constructive reasons to allow the addition of a compressed air installation next to the intake gallery. Secondary air was injected between the TR1 and TR2 intake sections. The scale model of the gallery was made from the entrance of the 90-degree transition volute to the exit of the TR2 intake manifold. The gallery components were made of PLA [18-21] by 3D printing, and assembled by screws [22-24]. The side walls were made of plexiglass plates.
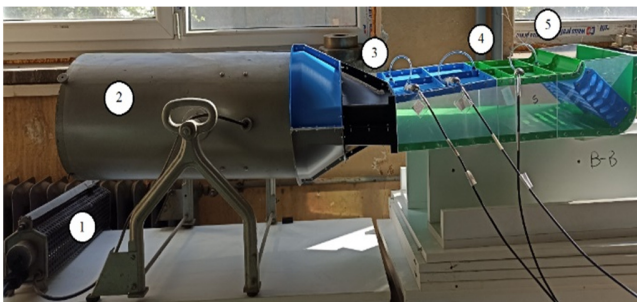

Fig. 13.   The 1:4 scale model of the original intake ducting: 1 - rheostat; 2 - axial fan; 3, 4, and 5 - pressure nozzles.

To determine the static pressure, the intake manifold was equipped with static pressure sockets, where the pressure sensors were connected. Pressure socket 1 was at the elbow exit (position 5), pressure socket 2 was at the exit of the section with constant section (position 4), and section 3 was at the exit from section 3 (position 3), respectively, at the entrance to the fan connection. To simulate the flow of the admission air of the gas turbine, a variable speed ducted fan was used, which was coupled to the scale model using a variable cross-section, with the inlet section from the rectangular shape (outlet from TR2) and the outlet section on the circular (entry into the ducted fan). This investigation aimed to determine a geometric configuration that allows air injection into the gas turbine intake manifold using linear nozzles arranged transversely to the gallery walls and to confirm the numerical models used for airflow calculation. The 1:4 scale model of the modified manifold contains a section to which two transverse linear nozzles are added, fed by cylindrical manifolds. The cylindrical

manifolds were supplied with pressurized air from the side of the experimental device having a total of four air intakes. Figure 14 shows the experimental setup, with the secondary air supply system mounted and connected to a compressor. Figure 15 shows the modified intake duct section with the direction of airflow located between TR1 and TR2, and the geometry of the manifold, linear nozzle, and manifold wall in the form of the NACA 0018 profile. The nozzle exit position is downstream with 35 mm against minimal transversal area and the manifold channel and the angle of 30 degrees. The geometry of the collector gallery is cylindrical with a diameter of 12 mm and the angle between the walls of the nozzle is 8°.
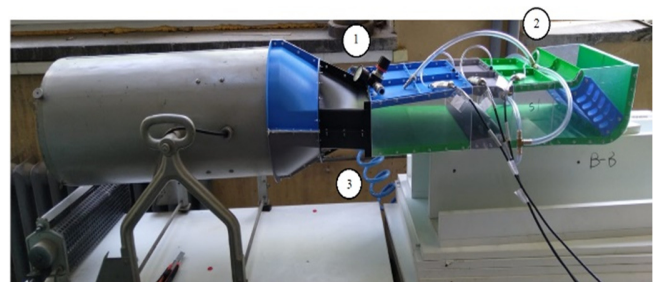

Fig. 14.   The 1:4 scale model of the modified intake ducting: 1 - pressure regulator; 2 - compressed air tubing system; 3 - compressed air main supply.
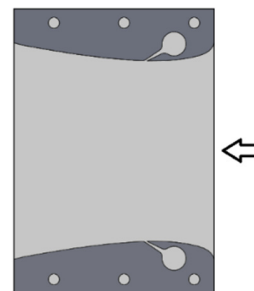

Fig. 15.   The modified intake ducting section with flow direction.

To determine static pressure, Kistler piezoresistive differential pressure sensors with a scale of ±10 kPa were used, which were connected (with the depression socket) to the pressure sockets provided by construction on the scale model. A Pitot tube connected to a pressure sensor described above was used to determine the speed. The useful length of the anemometer rod was 143 mm, and subtracting 3 mm of the thickness of the plexiglass side wall resulted in a measurement length of 140 mm from the side wall. Data acquisition was performed with the QuantumX MX1615B module. The device was used to acquire data from resistive, inductive, or piezoresistive strain gauge bridges in full-bridge, half-bridge, and quarter-bridge configurations. This device is also used for transducers, potentiometers, and resistance thermometers based on strain gauges. The module was equipped with 16 individually configurable sensor inputs. To determine the velocities, the Pitot tube was inserted into the intake manifold, its tip passing through lines 1, 2, and 3. Its position with respect to the reference system was: line 1 at $x = 155$ mm, line 2 at $x = 387$ mm, and line 3 at $x = 572$ mm. For all lines, $y = 59$ mm relative to the coordinate system of Figure 16.
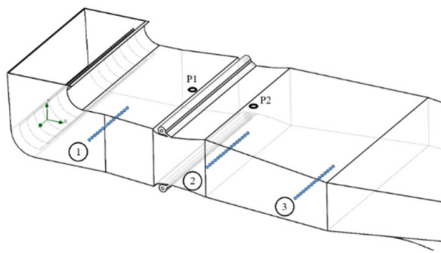
Fig. 16.   The measurement lines.

V.   RESULTS VERIFICATION AND VALIDATION

Figures 17-22 present the numerical and experimental speed variations for the three lines under the operating conditions of only the fan in the maximum operating mode, with a speed of 3000 rpm (experimental: red, numerical: blue, measured in 10 mm increments). The graphic representations in these Figures show that in the positioning domain of the z coordinate, there is a range where the agreement of the numerical results with the experimental ones is very good. The discrepancy outside this range, although sometimes quantitatively admissible, is caused by the end effects of the range considered.
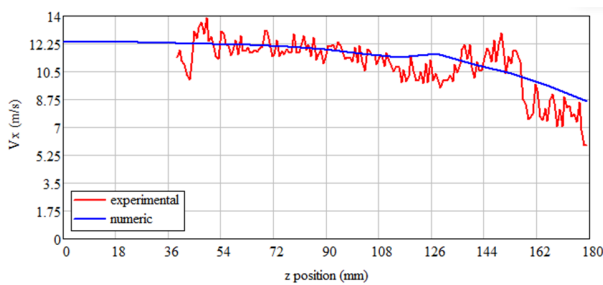

Fig. 17.   Speed variation on line 1 on the original gallery model.
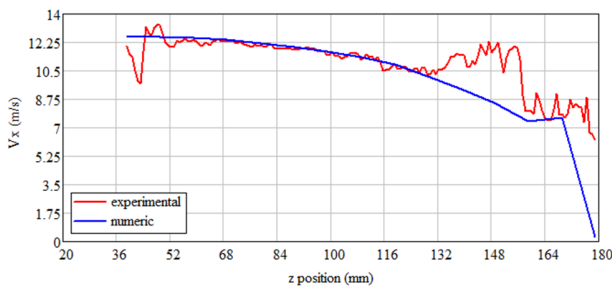

Fig. 18.   Speed variation on line 1 on the modified gallery model.
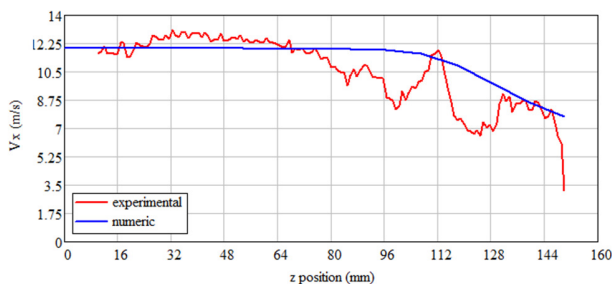

Fig. 19.   Speed variation on line 2 on the original gallery model.
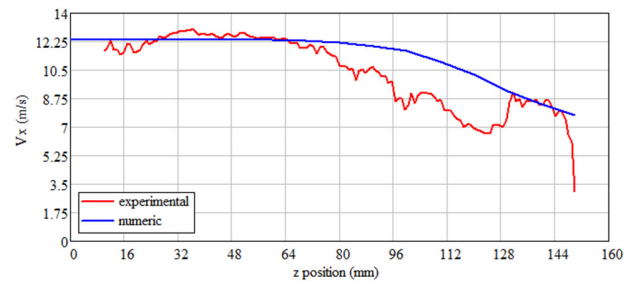

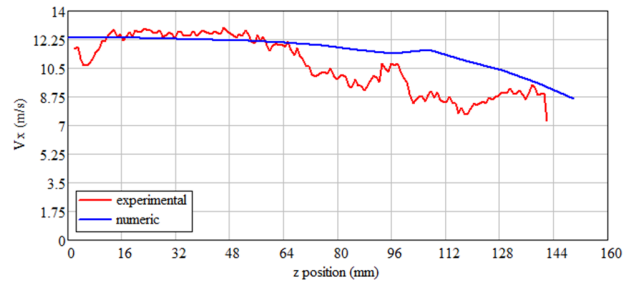Fig. 20.   Speed variation on line 2 on the modified gallery model.

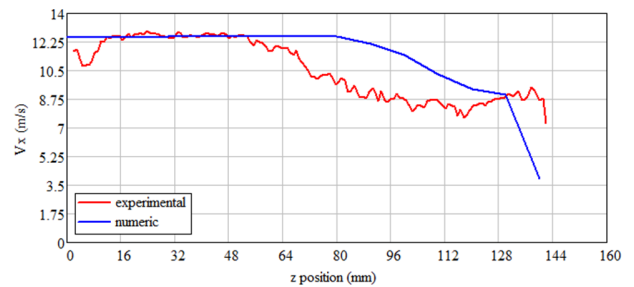Fig. 21.   Speed variation on line 3 on the original gallery model.

Fig. 22.   Speed variation on line 3 on the modified gallery model.

VI.   CONCLUSIONS

The concordance of the numerical and experimental results obtained on the model with the modified section validates both the applied solution and the correctness of the numerical modeling. The differences noted in the streamlines are noticeable in the vertical plane, especially after exiting the modified section, in the area located in the vicinity of the plane of symmetry. It was found that for the geometrical configuration considered, using the secondary air injection in the scale model of the gallery section, an additional flow rate of about 7 times higher than the injected flow rate is created at the entrance to the gallery. These results were obtained numerically, under steady flow conditions and for a path shorter than the original gas turbine inlet manifold path, with lower pressure losses, for a 1:4 scale model.

For all geometric configurations considered, in the case of secondary air injection, after exiting the intake manifold nozzle, there is a tendency to concentrate the airflow toward the plane of symmetry of the manifold. Numerical calculations showed a decrease in airflow at the gallery outlet with an increase in the distance from the leading edge of the wall of the modified section to the linear nozzle, according to the first-order regression function. According to this observation, the

maximum effect was obtained for the exit of the nozzle in the turbine intake manifold according to the minimum section of the modified section, at $x = 30$ mm. The quadratic regression function has a maximum at $x = 44.24$ mm. Since these values are indicative, a value in this range can be adopted for the outlet of the nozzle in the gallery. Increasing the angle of inclination of the linear nozzle relative to the horizontal leads to an airflow decrease at the gallery outlet. Both regression laws indicate this, the maximum of the second-order regression being at the tilt angle of approximately 10°, which is practically impossible to achieve. For constructive reasons, an angle of 30° can be adopted. For values lower than this, the manifold is very close to the body of the intake manifold. Therefore, it was assumed that the experimental results confirmed the numerical results for the airflow produced by the fan, both for the scale model of the original gallery and for the scale model of the gallery with the modified section. The differences between the measured velocity values and the experimental ones are mainly due to the positioning error of the anemometer and the alteration of the measurement in the vicinity of the gallery walls. The directions in which the velocities were measured are located in the middle of the gallery, noting the existence of small differences in the velocity profile for the two configurations. This study aimed to constitute a validated method and model, with a high degree of generality for other similar situations.

REFERENCES

[1] T. Giampaolo, *Gas Turbine Handbook: Principles and Practice, Fifth Edition*, 5th ed. New York, NY, USA: River Publishers, 2020.

[2] "The Twin TF Marine Gas Turbine Propulsion Package: The Solution for High Performance," *Vericor*. https://www.vericor.com/success-stories/the-twin-tf-marine-gas-turbine-propulsion-package-the-solution-for-high-performance/.

[3] M. Wilcox, R. Baldwin, A. Garcia-Hernandez, and K. Brun, "Guideline for gas turbine inlet air filtration systems," Gas Machinery Research Council - Southwest Research Institute, Apr. 2010.

[4] G. I. Balan, O. N. Volintiru, I. C. Scurtu, F. Ioniță, M. L. Vasile, and C. Borzea, "Considerations regarding the anti-icing system for the ship propulsion plant with gas turbine," *E3S Web of Conferences*, vol. 286, 2021, Art. no. 04013, https://doi.org/10.1051/e3sconf/202128604013.

[5] F. Niculescu, M. L. Vasile, G. Balan, A. Săvescu, and R. Nicolae, "Virtual Indication of the Torque for a Marine Gas Turbine | Technium: Romanian Journal of Applied Sciences and Technology," *Technium: Romanian Journal of Applied Sciences and Technology*, vol. 3, no. 10, pp. 74–81, Nov. 2021, https://doi.org/10.47577/technium.v3i10.5140.

[6] I. Vlăducă *et al.*, "Automation Control System for Naval Propulsion Retrofitting," in *2021 International Conference on Applied and Theoretical Electricity (ICATE)*, Craiova, Romania, Feb. 2021, pp. 1–6, https://doi.org/10.1109/ICATE49685.2021.9465065.

[7] N. Aye, G. McAndrews, and B. Mendenhall, "Marine Gas Turbine Package for the Korean Navy PKX Program," presented at the ASME Turbo Expo 2008: Power for Land, Sea, and Air, Berlin, Germany, Aug. 2009, pp. 387–394, https://doi.org/10.1115/GT2008-50098.

[8] P. Sun, H. Gao, J. Zhong, and M. Yang, "Aerodynamic Performance Investigation of Modern Marine Gas Turbine Intake System," presented at the ASME Turbo Expo 2012: Turbine Technical Conference and Exposition, Copenhagen, Denmark, Jul. 2013, pp. 367–373, https://doi.org/10.1115/GT2012-69694.

[9] T. Zierer and B. Matyschok, "Design, Development and Verification of Gas Turbine GT24 Air Intake," presented at the ASME 1997 Turbo Asia Conference, Singapore, Dec. 2014, https://doi.org/10.1115/97-AA-009.

[10] E. Avram, V. Nastasescu, and G. Malos, *Metoda Elementelor Finite in Mecanica Fluidelor*. Bucharest, Romania: Editura Academiei Tehnice Militare, 2003.

[11] S. Stefan and V. Nastasescu, *Simularea fenomenelor mecanice şi hidraulice*. Bucharest, Romania: Editura Academiei Tehnice Militare, 2000.

[12] G. Balan, *Aerogazodinamica*. Chisinau, Moldova: Technica-Info, 2003.

[13] "Heating, Ventilating, and Air-Conditioning Applications," ASHRAE, Atlanta, GA, USA, 2019.

[14] V. Nastasescu, "The Using of the Multilayer Plate Concept in the Calculus of Functionally Graded Plates," *Applied Sciences*, vol. 12, no. 21, 2022, https://doi.org/10.3390/app122110695.

[15] V. Nastasescu, A. Stefan, and C. Lupoiu, *Analiza neliniară a structurilor mecanice prin metoda elementelor finite*. Bucharest, Romania: Editura Academiei tehnice Militare, 2002.

[16] P. K. Kundu and I. M. Cohen, *Fluid Mechanics*, 4th ed. Burlington, MA, USA: Academic Press.

[17] D. C. Rennels and H. M. Hudson, *Pipe Flow: A Practical and Comprehensive Guide*, 1st ed. Wiley, 2012.

[18] D. G. Zisopol, I. Nae, and A. I. Portoaca, "Compression Behavior of FFF Printed Parts Obtained by Varying Layer Height and Infill Percentage," *Engineering, Technology & Applied Science Research*, vol. 12, no. 6, pp. 9747–9751, Dec. 2022, https://doi.org/10.48084/etasr.5488.

[19] D. G. Zisopol, A. I. Portoaca, I. Nae, and I. Ramadan, "A Comparative Analysis of the Mechanical Properties of Annealed PLA," *Engineering, Technology & Applied Science Research*, vol. 12, no. 4, pp. 8978–8981, Aug. 2022, https://doi.org/10.48084/etasr.5123.

[20] D. G. Zisopol, I. Nae, A. I. Portoaca, and I. Ramadan, "A Statistical Approach of the Flexural Strength of PLA and ABS 3D Printed Parts," *Engineering, Technology & Applied Science Research*, vol. 12, no. 2, pp. 8248–8252, Apr. 2022, https://doi.org/10.48084/etasr.4739.

[21] D. G. Zisopol, I. Nae, A. I. Portoaca, and I. Ramadan, "A Theoretical and Experimental Research on the Influence of FDM Parameters on Tensile Strength and Hardness of Parts Made of Polylactic Acid," *Engineering, Technology & Applied Science Research*, vol. 11, no. 4, pp. 7458–7463, Aug. 2021, https://doi.org/10.48084/etasr.4311.

[22] D. G. Zisopol, A. I. Portoaca, and M. Tanase, "Improving the Impact Resistance through Annealing in PLA 3D Printed Parts," *Engineering, Technology & Applied Science Research*, vol. 13, no. 5, pp. 11768–11772, Oct. 2023, https://doi.org/10.48084/etasr.6281.

[23] D. G. Zisopol, A. I. Portoaca, and M. Tanase, "Dimensional Accuracy of 3D Printed Dog-bone Tensile Samples: A Case Study," *Engineering, Technology & Applied Science Research*, vol. 13, no. 4, pp. 11400–11405, Aug. 2023, https://doi.org/10.48084/etasr.6060.

[24] D. G. Zisopol, N. Ion, and A. I. Portoaca, "Comparison of the Charpy Resilience of Two 3D Printed Materials: A Study on the Impact Resistance of Plastic Parts," *Engineering, Technology & Applied Science Research*, vol. 13, no. 3, pp. 10781–10784, Jun. 2023, https://doi.org/10.48084/etasr.5876.